ChemPubSoc Europe

DOI: 10.1002/cplu.201900181

CHEMPLUSCHEM Full Papers

SPECIAL ISSUE

Multivalency in Heteroternary Complexes on Cucurbit[8]uril-Functionalized Surfaces: Self-assembly, Patterning, and Exchange Processes

Virginia Valderrey[+,a] Maike Wiemann[+,b] Pascal Jonkheijm,*[b] Stefan Hecht,*[a] and Jurriaan Huskens*[b]

The spatial confinement of multivalent azopyridine guest molecules mediated by cucurbit[8]urils is described. Fluorescent dye-labelled multivalent azopyridine molecules were attached to preformed methyl viologen/cucurbit[8]uril inclusion complexes in solution and at surfaces. The formation of the resulting heteroternary host–guest complexes was verified in solution and on gold substrates. Surface binding constants of the multivalent ligands were two orders of magnitude higher than that of the monovalent one. Poly-L-lysine grafted with oligo(ethylene glycol) and maleimide moieties was deposited on cyclic olefin polymer surfaces and further modified with thiolated methyl viologen and cucurbit[8]uril. Defined micrometer-sized patterns were created by soft lithographic techniques. Supramolecular exchange experiments were performed on these surface-bound heterocomplexes, which allowed the creation of cross-patterns by taking advantage of the molecular valency, which led to the substitution of the monovalent guest by the multivalent guests but not vice versa.

Introduction

Engineered micropatterned surfaces are incorporated frequently in chemical or biological sensors, and therefore the development of new approaches for their construction is of high interest.[1] The assembly of molecules on surfaces by means of non-covalent interactions is widely employed due to the specificity, controlled affinity, and reversibility of these interactions.[2,3] Multivalency allows to tune the binding strength of those non-covalent assemblies by combining several individual interactions, resulting in concomitant increase in affinity as well as thermodynamic and kinetic stability of the complexes on surfaces.[4,5] We have described multivalent systems on surfaces, mainly using adamantane β-cyclodextrin host-guest complexes.[3,5–8] Our results have shown an increase in binding affinity over several orders of magnitude resulting from the multivalent use of this interaction motif. This change in affinity also affects the dynamics of the surface-bound complex with increasing number of binding sites, going from a reversibly bound guest to a stable, kinetically trapped guest.[4,5]

The position of molecules on a surface in a precise manner can be achieved by using so-called soft lithography techniques.[9–14] The fabrication of two-component microarrayed polymers,[15] particles,[16] carbohydrates,[17] and proteins,[18,19] is mostly achieved using advanced lithographic technologies. Chemically modified bifunctional surfaces can be used to achieve cross patterns.[20,21] In most of these examples, the assembly of guest molecules with a host-functionalized surface is achieved by the formation of binary complexes. Examples involving ternary complexes are, however, more scarce.[22–24] At the same time, the necessity of a third molecule to form the assembly offers new ways to control the density, affinity, reversibility, and dynamics of the assembled complexes. Cucurbit[8]uril (CB[8]) is well-known for the ability to form ternary complexes.[25,26] CB[8] binds electron-deficient methyl viologen with an association constant, K, of 10^5–10^6 M^{-1}, and the resulting methyl viologen⊂CB[8] complex can efficiently include a second electron-rich aromatic guest. These ternary complexes were already used to selectively adhere cells, bacteria or proteins to surfaces and releasing them on demand.[27–33]

Multivalent CB[8]-based host-guest complexes have been studied in solution and have been mainly based on polymeric scaffolds.[34,35] Here, we investigate the suitability of azopyridine guests for ternary complexation with CB[8] in solution and different types of surfaces, by using ^{1}H-NMR, isothermal titration calorimetry (ITC), surface plasmon resonance (SPR) spectroscopy, and quartz crystal microbalance with dissipation monitoring (QCM-D) for analysis. After verification of heteroternary

[a] Dr. V. Valderrey,[+] Prof. S. Hecht
Department of Chemistry & IRIS Adlershof
Humboldt-Universität zu Berlin
12489 Berlin (Germany)
E-mail: sh@chemie.hu-berlin.de

[b] Dr. M. Wiemann,[+] Prof. P. Jonkheijm, Prof. J. Huskens
Molecular Nanofabrication Group, MESA[+] Institute for Nanotechnology,
Department of Science and Technology
University of Twente
P.O. Box 217, 7500 AE Enschede (The Netherlands)
E-mail: p.jonkheijm@utwente.nl
j.huskens@utwente.nl

[+] These authors contributed equally to this work

Supporting information for this article is available on the WWW under https://doi.org/10.1002/cplu.201900181

This article is part of a Special Issue on "π-Conjugated (Macro)molecules and their Applications".

complex formation on the surface, the binding enhancement due to multivalency has been studied in detail and investigated by fluorescence microscopy. Microcontact printing and micromolding in capillaries (μCP and MIMIC) have been used as patterning techniques, offering high versatility and compatibility on the sub-micrometer level.[36] The combination of multivalent binding and these surface patterning techniques, allowed us to create cross-patterns of multivalent azopyridine molecules on methyl viologen⊂CB[8]-based self-assembled monolayers (SAMs), which is indicative for enhanced binding.

Results and Discussion

The synthesis of the photoswitchable azopyridine scaffold was performed according to described procedures.[37,38] Subsequently, the azopyridine unit was functionalized with a tetra (ethylene glycol) chain, which provides water solubility, resulting in molecule **1** (Figure 1).[31] Dimeric and trimeric azopyridine molecules were synthesized by the initial functionalization of **1** through ring-opening of succinic anhydride, followed by reaction of the corresponding carboxylic acids with either *N*-Boc-serinol or Boc-protected aminotris(hydroxymethyl)-methane, to obtain dimeric and trimeric azopyridine molecules, respectively. The following Boc-deprotection of these multivalent azopyridines with trifluoroacetic acid provided the corresponding trifluoroacetates **2** and **3**. Monovalent rhodamine- and fluorescein-functionalized azopyridines **5a** and **5b** were formed via an esterification reaction of **1** with rhodamine B and the addition of glycine-substituted **1** to fluorescein isothiocyanate, respectively. Treatment of molecules **2** and **3** with base followed by reaction with fluorescein isothiocyanate, afforded the fluorescein-labelled dimer **6** and trimer **7**. Gold or polymeric surfaces were functionalized (processes described below) with the thiol-substituted methyl viologen derivative **4b**, which was synthesized as previously reported in the literature (Figure 1).[38] Additional details of the synthetic procedures have been described in the Supporting Information.

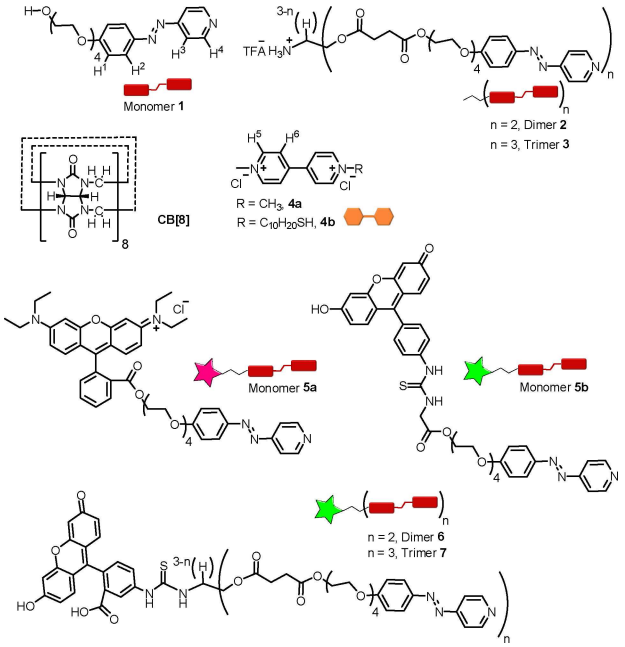

Figure 1. Chemical structures of the azopyridine derivatives with different valences **1**, **2**, and **3**, methyl viologen derivatives **4a** and **4b**, CB[8] macrocycle and rhodamine/fluorescein-labelled azopyridine monomers **5a** and **5b** and multivalent azopyridines **6** and **7** used in this study.

The formation of the heteroternary complex **1**·**4a**⊂CB[8] in aqueous solution was initially studied by ^{1}H-NMR titration experiments (Figure 2a, Figure S1 in the Supporting Information).

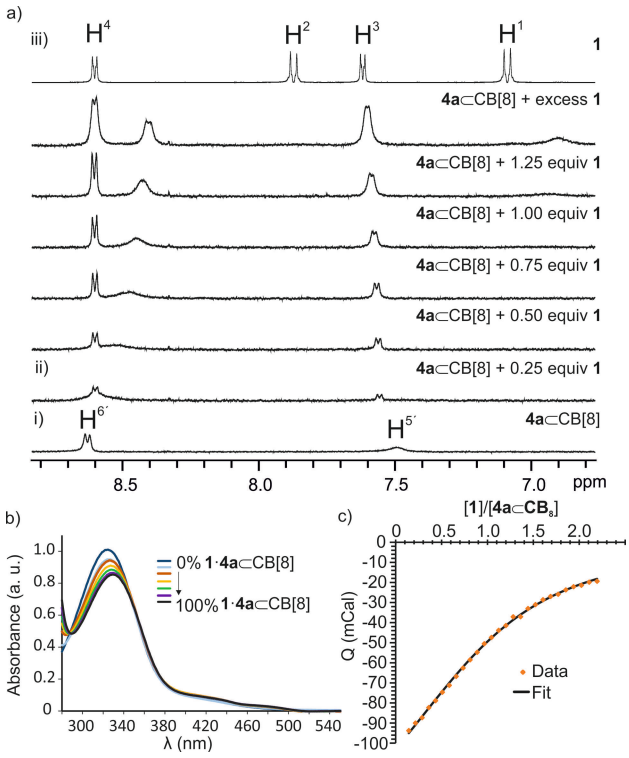

Figure 2. a) Aromatic region of the ^{1}H-NMR spectra (D_2O, 298 K, 500 MHz) of i) an equimolar mixture of **4a**⊂CB[8], ([**4a**⊂CB[8]] = 1.4×10^{-4} M), ii) increasing quantities of **1** (0-approximately 2 equiv) and iii) pure **1**. Numbers with primes indicate complex formation. See Figure 1 for proton assignment. b) UV/Vis spectra of **1** (PBS, [**1**] = 5×10^{-5} M) upon addition of increasing quantities of the preformed inclusion complex **4a**⊂CB[8] (molar ratio from 0 to 100%). c) Isothermal calorimetric data obtained in the titration of a PBS solution of **4a**⊂CB[8] by adding increments of the azopyridine monomer **1**. [CB[8]] = [**4a**] = 0.1 mM, [**1**] = 1.0 mM.

tion). Upon addition of increasing quantities of **1** to a 0.1 mM solution of **4a**⊂CB[8] in PBS, slight upfield shifts for the aromatic proton signals of **4a** as compared to the previously formed 1:1 complex **4a**⊂CB[8] were observed.

Moreover, the aromatic proton signals of the azopyridine **1** became broad and upfield-shifted as compared to free **1** in solution, most likely due to formation of the heteroternary complex (Figure 2a). The joint upfield shift of both the aromatic protons of **4a** and of the azopyridine can be explained by the shielding effect from water caused by the inclusion of the guests in the hydrophobic pocket of the cucurbituril, as well as the π donor-acceptor interaction occurring between the two

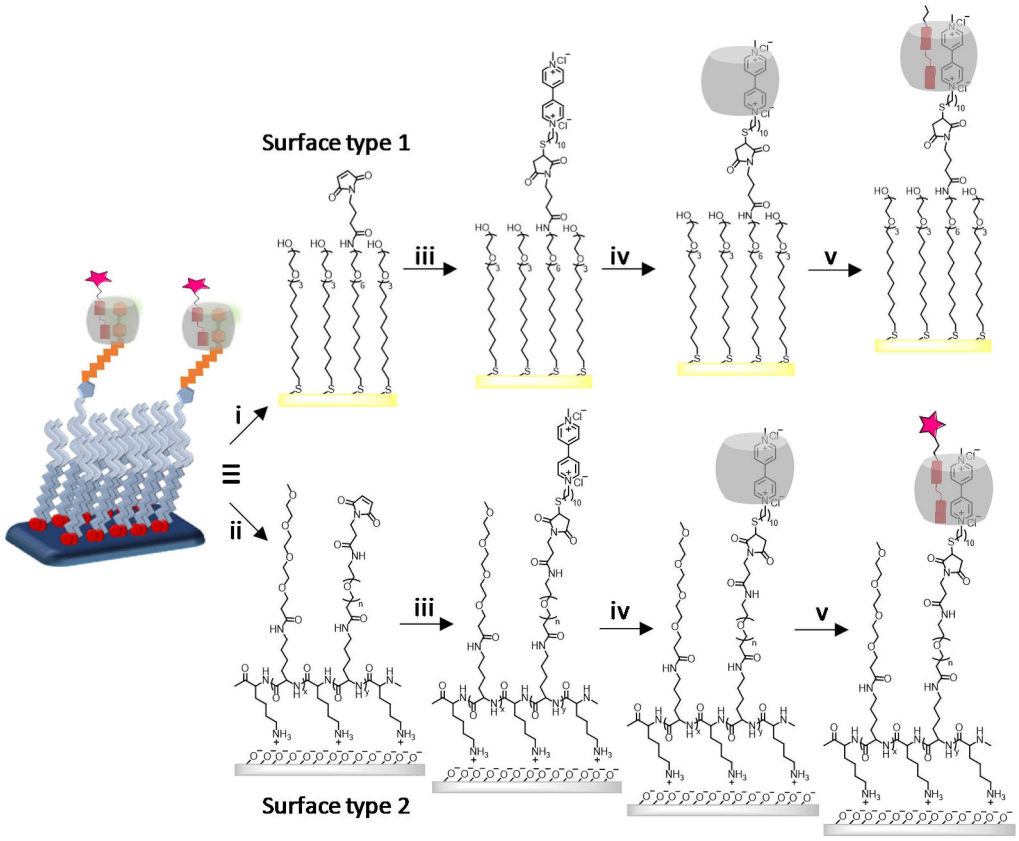

Scheme 1. Schematic outline of CB[8] layer formation on gold (type 1) and COP (type 2) surfaces and heteroternary complex formation. Assembly starts with i) overnight incubation of the disulfide-OEG/disulfide-OEG-Mal (surface type 1) in EtOH at rt, ii) PLL-OEG-Mal ($n=4$, $x=20\,\%$, $y=3\,\%$) incubation on oxygen plasma-activated COP (surface type 2) in PBS for 5–10 min at rt, iii) functionalization with **4b** for 1 h, iv) incubation with 50 μM CB[8] and v) assembly of a the azopyridine derivatives **1**, **2** and **3** (surface type 1) and fluorescence-labelled azopyridine derivatives **5**–**7** (surface type 2).

aromatic guest moieties. These results are in agreement with the previously reported formation of analogous complexes involving other azobenzene molecules.[22] Two-dimensional ^{1}H-NMR experiments also supported the formation of the heteroternary inclusion complex (Figure S2) as evidenced by the NOE cross-peaks between the protons of **4a** and the aromatic protons of the azopyridine moiety of **1**. The interaction of azopyridine **1** with the inclusion complex **4a**⊂CB[8] was further confirmed by UV/Vis titration experiments. Upon addition of **4a**⊂CB[8], a decrease in the absorbance accompanied with a red-shift of the $\pi\rightarrow\pi^*$ band of **1** was observed. An isosbestic point at around 365 nm indicates the formation of a new supramolecular species that we ascribe to the ternary complex **1**·**4a**⊂CB[8] (Figure 2b). The intrinsic binding constant for the formation of the heteroternary inclusion complex with the monomer **1** was estimated using ITC experiments (Figures 2c and S3). An equimolar mixture containing the preformed **4a**⊂CB[8] complex ([**4a**⊂CB[8]]$=0.1$ mM) was titrated with a solution of **1** ([**1**]$=1.0$ mM) in PBS. The observed exothermic binding curve has an inflection point at a molar ratio of one indicating the formation of a 1:1 assembly. The data fitting of the titration to a 1:1 binding model gave an association constant $K_{\mathbf{1}\cdot\mathbf{4a}\subset CB[8]}=(1.7\pm0.1)\times10^4\ M^{-1}$, in line with values found for similar complexes.[33]

Surface experiments were performed on two different types of surfaces depicted in Scheme 1 (experimental details given in Supporting Information). The first type of surface consists of a mixed SAM of thiols on gold (surface type 1, Scheme 1, top). Type 1 surfaces were fabricated by incubation of gold sensors with a mixture of antifouling oligo(ethylene glycol) alkanethiols, 1 % of which contained a maleimide group.[39,40] Surfaces of type 2 were fabricated on cyclic olefin polymer (COP) platforms coated with a SAM of poly-L-lysine grafted with 20 % oligo (ethylene glycol) and 3 % maleimide-oligo(ethylene glycol) (PLL-OEG-Mal). For COP substrates (surface type 2), the surface was exposed to oxygen plasma to assure good surface wettability and electrostatic adhesion of PLL-OEG-Mal to the COP substrates[41] (see Scheme 1 ii). The electrostatic adsorption of the PLL-OEG-Mal was monitored with QCM-D (Figure S4). The maleimide moieties of type 1 and type 2 surfaces were then functionalized by a Michael addition with thiol-substituted methyl viologen **4b**. Successful immobilization of CB[8] and the formation of ternary complexes on those surfaces has been verified by QCM-D control experiments (Figures S5 and S6) and revealed results comparable to previously reported examples.[33]

The stepwise formation of the different layers was monitored by water contact angle goniometry (see Supporting Information for more details, Figure S7). A change in the

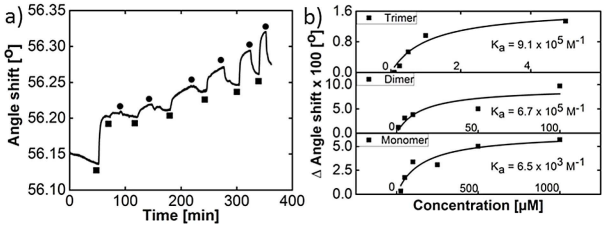

Figure 3. a) SPR sensogram of a titration on a type 1 surface of **4b**⊂CB[8] with monomer **1**; starting with i) CB[8] (50 μM) adsorption, followed by the concentration-dependent interaction of **1** (25, 50, 100, 250, 500, 1000 μM), depicted by squares (▪) and ii) subsequent rinsing steps with 100 μM **4a**⊂CB[8] depicted by circles (•). b) Change in angle shift *vs* concentration of the multivalent azopyridines: monomer **1**, dimer **2** and trimer **3** (1:1 Langmuir fits are shown) according to their SPR sensograms where K_a is the estimated association constant.

polarity of the surface was observed after the functionalization of the oxygen plasma-activated surface with PLL-OEG-Mal. The water contact angle increased from 8.0° to 29.7°, which agrees with other PLL-modified substrates.[42,43] The water contact angle increased even more, up to 41.0°, upon the functionalization of the PLL-OEG-Mal with **4b**. To support retention of the host-guest binding properties of the surface-bound methylviologen groups, the PLL-OEG-**4b** layer was incubated with CB[8], upon which the water contact angle reached 54.0°.

To confirm the formation of the complexes on surfaces, we performed SPR and QCMD titrations. SPR sensograms for the reversible formation of the ternary complex on a **4b**-functionalized SAM (surface type 1) are depicted in Figure 3a. Initially, the SPR angle change was measured after the binding of pure CB[8] in water, and this change was in agreement with previously described measurements.[44] Subsequently, aqueous solutions containing CB[8], ([CB[8]] = 50 μM) and increasing concentrations of **1** (ranging from 0.025 to 1.0 mM) were added resulting in different increases of the SPR angle directly related with the sample concentration and proving adsorption on the surface. After reaching signal saturation at each concentration of **1**, the system was equilibrated for approx. 10 min, and then the desorption of bound **1** was performed by rinsing the system with a 100 μM solution of **4a**⊂CB[8] until the system reached saturation again. Finally, the change of the SPR angle at each concentration of **1** was used to derive the equilibrium binding constant for the formation of the heteroternary complex on the gold surface as $K_{\mathbf{1}\cdot\mathbf{4b}\subset CB[8]} = 6.5\times10^3\ M^{-1}$ (Figure 3b, Figure S8). This binding constant is similar to the one estimated in solution, indicating that the thermodynamic stability of the monovalent heteroternary complex in solution and on the gold surface is, as expected, comparable.

In order to form more stable complexes and to gain insight into the effect of multiple azopyridine binding units on the overall stability of these supramolecular assemblies, we performed similar surface binding experiments with bi- and trivalent azopyridines (Figures S9 and S10). SPR measurements were performed in a similar manner as the ones described for the monovalent system (*vide supra*). After adding increasing concentrations of **2** to the system (ranging from 0.002 mM to 0.1 mM) the overall estimated binding constant was $K_{\mathbf{2}\cdot\mathbf{4b}\subset CB[8]} = 6.7\times10^5\ M^{-1}$ (Figure S9). This value is two orders of magnitude higher than the one of the monovalent interaction on the same type of platform confirming that both azopyridine units are involved in binding to the platform. The binding constant of **3** ($K_{\mathbf{3}\cdot\mathbf{4b}\subset CB[8]} = 9.1\times10^5\ M^{-1}$) is of the same order of magnitude as the one of **2**, which suggests that (only) bivalent binding prevails for binding the trivalent guest to the **4b**⊂CB[8] SAM (Figure S10). Mismatches between the steric requirements to bind all three guest moieties of the trivalent guest to the surface may be a possible explanation for the lower than expected binding affinity and stoichiometry.

Once we confirmed the formation of the ternary complexes both in solution and on surfaces and showed that the di- and trivalent guests give a stronger binding affinity on the surface than the monovalent one, we investigated the lithographic patterning of the ternary molecular assemblies on duly functionalized cyclic olefin polymer (COP) surfaces, using fluorescence microscopy as the read-out method. To this aim, the fluorescent molecules **5**, **6**, and **7** were used as guests. As platforms, COP surfaces were employed (Scheme 1, surface type 2) to avoid the well-known quenching effect that gold induces on the emission of fluorescence-labelled molecules adsorbed at distances below 50 nm of the surface.[45] COP substrates, modified with PLL-OEG-Mal and subsequently reacted with thiol-modified viologen **4b**, were incubated with a 50 μM solution of CB[8] to form the binary complex **4b**⊂CB[8] followed by the printing of the fluorescent guest molecules. Alternatively, the fluorescent guest was simultaneously adsorbed to the surface with CB[8], by using a solution that contained both molecules in a 1:5 (guest site:CB[8]) molar ratio to ensure heteroternary complex formation.

Microcontact printing (μCP) and micromolding in capillaries (MIMIC) were used to pattern the PLL-OEG-Mal-**4b**⊂CB[8]-modified COP (surface type 2) substrates with micrometer-scale structures. Polydimethylsiloxane (PDMS) stamps were adequately cut and used following standard procedures[46,47] for each lithographic technique. For μCP, (regular, non-treated) PDMS stamps were inked for 15 min with a 10 μM aqueous solution of the respective fluorescent guest and placed into contact with the CB[8]-functionalized COP substrates for 5 min. After removing the stamp and rinsing with water, fluorescence microscopy images were recorded (Figure 4).

For MIMIC experiments, the PDMS stamps were placed with the channels facing the surface, and conformal contact between the PDMS stamp and the COP surface was ensured. For this technique PDMS stamps with channels were filled, driven by capillary forces, with a 10 μM solution of the fluorescent guest, which was allowed to incubate for 5 min. After removing the stamp and rinsing with water, fluorescence microscopy images were recorded (Figure 5).

To prove that the fluorescent patterns were exclusively formed due to the specific interaction between the fluorescent guest and the inclusion complex **4b**⊂CB[8] on the COP surface, several control experiments were performed (Figures S11–S13). These experiments were performed following the above described procedures of μCP and MIMIC. After each incubation step the azopyridine guest was incubated on the corresponding

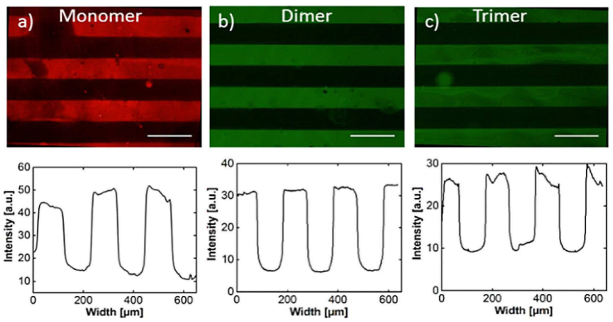

Figure 4. Fluorescence microscopy images and corresponding intensity profiles of **4b**⊂CB[8]-functionalized COP surfaces (following the general functionalization procedure depicted in Scheme 1, surface type 2) after μCP of (a) rhodamine-labelled monomer **5a**, or fluorescein-labelled (b) dimer **6**, or (c) trimer **7**. In all the cases, inking of the (non-activated) stamps was performed with a 10 μM aqueous ink solution, and contact was applied for 5 min. (Scale bars 200 μm. Imaging setting ISO400, 100% light intensity).

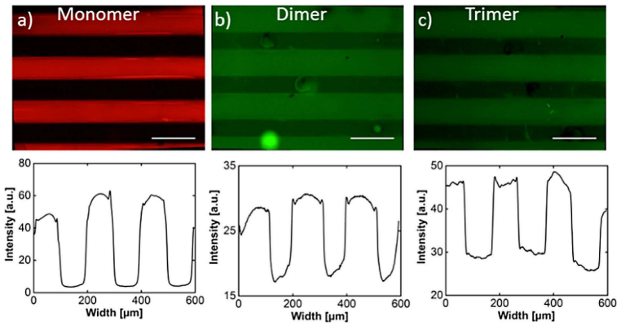

Figure 5. Fluorescence microscopy images and corresponding intensity profiles of **4b**⊂CB[8]-functionalized COP surfaces following the general functionalization procedure depicted in Scheme 1 (surface type 2), after MIMIC (inking time 5 min) of (a) rhodamine-labelled monomer **5a**, or fluorescein-labelled (b) dimer **6** or (c) trimer **7**. (Scale bars 200 μm. Imaging setting ISO400, 100% light intensity).

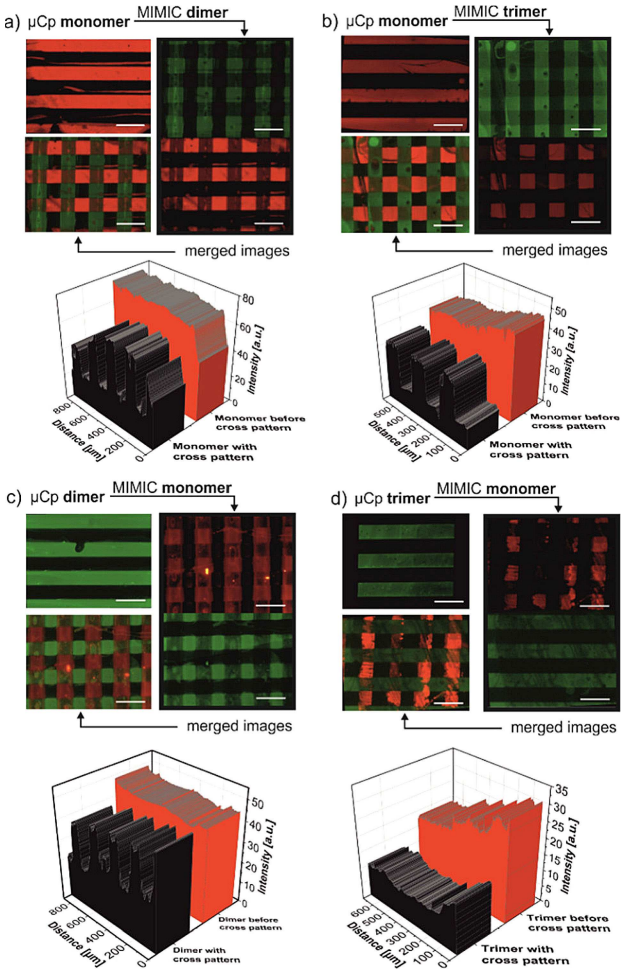

Figure 6. a) Fluorescence microscopy images of surface type 2 substrates patterned by μCP of monomer **5a**, followed by MIMIC of dimer **6**, merged channels, and **5a** after substitution by **6**. Below corresponding intensity profile of **5a** before and after MIMIC deposition of **6**. b) Fluorescence microscopy images of μCP monomer **5a**, MIMIC trimer **7**, merged channels, and **5a** after substitution by **7**. Below corresponding intensity profile of **5a** before and after MIMIC deposition of 7. c) Fluorescence microscopy images of μCP dimer **6**, MIMIC monomer **5a**, merged channels, and **6** after deposition of **5a**. Below corresponding intensity profiles of **6** before and after MIMIC of **5a**. d) Fluorescence microscopy images of μCP trimer **7**, MIMIC monomer **5a**, merged channels, and **7** after deposition of **5a**. Below corresponding intensity profile of **7** before and after MIMIC of **5a**. The height profiles have been measured along the longitudinal stripes. (Scale bar 200 μm. Imaging setting ISO400, 100% light intensity).

layer and evaluated regarding nonspecific interactions. Nonspecific interactions were observed with complementary charged surface components, but distinct patterns were observed on surfaces where CB[8] was present. With both, μCP and MIMIC, azopyridine guests were printed on **4b**⊂CB[8]-modified COP surfaces resulting in patterns without considerable nonspecific interactions. Generally, the incubation of rhodamine-functionalized guests gave less background fluorescence compared to fluorescein-labelled guests, which is tentatively explained by electrostatic interaction of the fluorescein dye with other complementary surface components. Furthermore, MIMIC deposition led to patterns with different intensity contrasts compared to μCP patterns. One explanation for that issue could be a higher amount of fluorescently labelled material introduced to the surface during the MIMIC step. Rinsing with water (for 5 min) after patterning did not lead to a significant desorption from the surface, neither for the monomer **5a** nor the multivalent guests **6** and **7**, indicating that the patterns are indeed stable.

Finally, we were interested to explore how the different valencies of the fluorescent guests can be used to fabricate more complex cross-patterns. The assembly of two differently fluorescently labelled guest molecules in an orthogonal fashion resulted in fluorescent cross-patterns, which were produced via two sequential deposition steps. In the initial step, a first guest was patterned using microcontact printing (Figure 6, left top panels, horizontal lines) according to the procedure explained above. In the subsequent step, a second guest was deposited, using MIMIC (for 5 min), on top of and orthogonal to the line patterns of the first guest (Figure 6, in vertical lines). Hereto, a second PDMS stamp was placed perpendicular on the same COP surface, and the contact of the solution with the second guest, delivered through the PDMS channels of the MIMIC stamp, provided competition between the first and second

guest in the cross-patterned areas. This procedure allowed us to observe clear cross-patterns of monovalent and multivalent molecules functionalized with different fluorophores (Figure 6). The cross-patterns appeared as a result of competition between the first and second guest in the areas where exchange was possible. The line pattern of monomer **5a** followed by the line pattern after perpendicular patterning of dimer **6** and trimer **7** is shown in Figures 6a and 6b. Both images show a checkerboard pattern after the second incubation step, which we attribute to a lower coverage of monomer **5a**. When the order of guest incubation was reversed, *i.e.*, the stronger interacting guest by μCP followed by MIMIC of the lower affinity monomer **5a**, we expected only marginally diminished fluorescence intensities of dimer **6** and trimer **7** before and after deposition of monomer **5a**. Figure 6c has also a checkerboard pattern, but green fluorescence of dimer **6** remained visible, which is indicative for remaining divalent complexes at the surface. No checkerboard pattern was observed after deposition of the monomer **5a** onto the trimer **7** (Figure 6d). However, red fluorescence was observed partially due to physisorbed molecules on top of surface-bound trimer **7** (Figure 6d).

Based on the results presented above in mind, showing that rinsing does not lead to desorption from the surface (at least over a timeframe of 5 min), we can conclude that the exchange process, which does occur at this timescale, is guest-driven.[48] This competition between the surface-bound molecules that are occupying the **4b**⊂CB[8] binding cavities and molecules in solution introduced during the MIMIC step appears to be in favor of those with the higher valency since they are able to form thermodynamically more stable complexes on the surface. This is also supported by the reverse experiments, where no exchange was observed upon the deposition of multivalent guests first followed by monomer **5a**.

Thus, we can employ the enhanced stability of multivalent guests compared to monovalent guests in patterning and exchange processes to obtain well-defined areas using the ternary CB[8] complexes as the interaction motif.

Conclusion

We have demonstrated that heteroternary complexes can be successfully formed in solution and on self-assembled surfaces providing complexes with similar binding strengths as in solution. The formation of multivalent heteroternary complexes involving dimeric and trimeric azopyridine guests was also achieved on gold surfaces, and the association constants estimated by SPR allowed us to quantify a binding enhancement of two orders of magnitude upon going from a monovalent to a divalent interaction. This demonstrates the efficiency of the use of multivalency to achieve the formation of thermodynamically highly stable complexes on CB[8] surfaces. Multivalent azopyridine molecules labelled with different fluorophores were used to create micrometer size patterns on **4b**⊂CB[8] functionalized antifouling SAMs on COP surfaces. Microcontact printing and micromolding in capillaries were used to self-assemble the multivalent fluorescent molecules on surfaces, and both lithographic methods proved to be adequate to produce clear and reproducible patterns on the micrometer scale. The different valency as well as fluorescence of the guests were exploited for the creation of cross-patterned surfaces. The enhanced binding of multivalent guests on CB[8] surfaces allowed us to deposit and to replace specific molecules in defined positions on these surfaces.

Overall, our surface-immobilized CB[8] ternary complexes can reversibly bind electron-rich guest molecules leading to appropriately tuned surface properties. In addition, the azopyridine molecules used here could function as photoswitches, potentially providing access to light-responsive patterned substrates. Such controlled reversibility and photoresponsive properties give rise to potential applications including sensor surfaces or reusable templates for compound detection. The usage of **4b**⊂CB[8] thus effectively maintains the material density on different types of surfaces and enhances the stability of the functional surface. These self-assembled COP platforms, compatible with fluorescence microscopy, can be used to develop photo-responsive smart surfaces where the diffusion of the fluorescent molecules can be controlled with light. Moreover, the formation of micrometer-sized fluorescent patterns with light is currently under development in our laboratories by taking advantage of the different thermal half-lives of azobenzene and azopyridine molecules.

Experimental Section

Experimental details of synthetic procedures and compound characterization, ITC experiments, surface preparation, SPR and QCM-D experiments, contact angle and fluorescent microscopy data of control experiments.

Acknowledgements

*V.V. is indebted to the Alexander von Humboldt Foundation for providing a postdoctoral fellowship. M.W. is supported by the Netherlands Organization for Scientific Research (NWO) (NWO-VIDI 723.012.106 to P.J.). Generous support by the German Research Foundation (DFG via SFB 765) is gratefully acknowledged. Emanuela Cavatorta and Almudena Marti Morant are acknowledged for the synthesis of thiolated methyl viologen (**4b**) and PLL-OEG-Mal, and Jacopo Movilli and Daniele Di Iorio are acknowledged for their helpful discussions.*

Conflict of Interest

The authors declare no conflict of interest.

Keywords: azopyridines · cucurbiturils · heteroternary complexes · host-guest complexation · multivalency

[1] A. Kumar, H. A. Biebuyck, G. M. Whitesides, *Langmuir* **1994**, *10*, 1498–1511.

[2] J. Huskens, M. A. Deij, D. N. Reinhoudt, *Angew. Chem. Int. Ed.* **2002**, *41*, 4467–4471, *Angew. Chem.* **2002**, *114*, 4647–4651.
[3] A. Mulder, S. Onclin, M. Peter, J. P. Hoogenboom, H. Beijleveld, J. ter Maat, M. F. Garcia-Parajo, B. J. Ravoo, J. Huskens, N. F. van Hulst, D. N. Reinhoudt, *Small* **2005**, *1*, 242–253.
[4] C. Fasting, C. Schalley, M. Weber, O. Seitz, S. Hecht, B. Koksch, J. Dernedde, C. Graf, E. W. Knapp, R. Haag, *Angew. Chem. Int. Ed.* **2012**, *51*, 10472–10498, *Angew. Chem.* **2012**, *124*, 10622–10650.
[5] A. Mulder, J. Huskens, D. N. Reinhoudt, *Org. Biomol. Chem.* **2004**, *2*, 3409–3424.
[6] J. Huskens, A. Mulder, T. Auletta, C. A. Nijhuis, M. J. W. Ludden, D. N. Reinhoudt, *J. Am. Chem. Soc.* **2004**, *126*, 6784–6797.
[7] A. Perl, A. Gomez-Casado, D. Thompson, H. H. Dam, P. Jonkheijm, D. N. Reinhoudt, J. Huskens, *Nat. Chem.* **2011**, *3*, 317–322.
[8] A. Gomez-Casado, H. H. Dam, M. D. Yilmaz, D. Florea, P. Jonkheijm, J. Huskens, *J. Am. Chem. Soc.* **2011**, *133*, 10849–10857.
[9] P. E. Laibinis, J. J. Hickman, M. S. Wrighton, G. M. Whitesides, *Science* **1989**, *245*, 845–847.
[10] J. J. Hickman, P. E. Laibinis, D. I. Auerbach, C. Zou, T. J. Gardner, G. M. Whitesides, M. S. Wrighton, *Langmuir* **1992**, *8*, 357–359.
[11] S. G. Im, K. W. Bong, B. S. Kim, S. H. Baxamusa, P. T. Hammond, P. S. Doyle, K. K. Gleason, *J. Am. Chem. Soc.* **2008**, *130*, 14424–14425.
[12] L. M. Demers, S. J. Park, T. A. Taton, Z. Li, C. A. Mirkin, *Angew. Chem. Int. Ed.* **2001**, *40*, 3071–3073, *Angew. Chem.* **2001**, *113*, 3161–3163.
[13] K. G. A. Tavakkoli, S. M. Nicaise, K. R. Gadelrab, A. Alexander-Katz, C. A. Ross, K. K. Berggren, *Nat. Commun.* **2016**, *7*, 10518–10529.
[14] L. Yang, A. Gomez-Casado, J. F. Young, H. D. Nguyen, J. Cabanas-Danes, J. Huskens, L. Brunsveld, P. Jonkheijm, *J. Am. Chem. Soc.* **2012**, *134*, 19199–19206.
[15] M. Park, C. Harrison, P. M. Chaikin, R. A. Register, D. H. Adamson, *Science* **1997**, *276*, 1401–1404.
[16] H. Xu, R. Hong, T. Lu, O. Uzun, V. M. Rotello, *J. Am. Chem. Soc.* **2006** *128*, 3162–3163.
[17] H. Sato, Y. Miura, N. Saito, K. Kobayashi, O. Takai, *Biomacromolecules* **2007** *8*, 753–756.
[18] K. M. Midthun, P. G. Taylor, C. Newby, M. Chatzichristidi, P. S. Petrou, J. K. Lee, S. E. Kakabakos, B. A. Baird, C. K. Ober, *Biomacromolecules* **2013**, *14*, 993–1002.
[19] D. Wasserberg, J. Cabanas-Danes, V. Subramnaniam, J. Huskens, P. Jonkheijm, *Chem. Commun.* **2018**, *54*, 1615–1618.
[20] L. Nebhani, C. Barner-Kowollik, *Adv. Mater.* **2009**, *21*, 3442–3468.
[21] D. A. Unruh, C. Mauldin, S. J. Pastine, M. Rolandi, J. M. Frechet, *J. Am. Chem. Soc.* **2010**, *132*, 6890–6891.
[22] F. Tian, D. Jiao, F. Biedermann, O. A. Scherman, *Nat. Commun.* **2012**, *3*, 1207–1215.
[23] J. Zhang, J. Liu, S. Chen, O. A. Scherman, C. Abell, *Adv. Funct. Mater.* **2018**, *28*, 1800550–1800557.
[24] C. Hu, Y. Lan, F. Tian, K. R. West, O. A. Scherman *Langmuir* **2014**, *30*, 10926–10932.
[25] S. J. Barrow, S. Kasera, M. J. Rowland, J. del Barrio, O. A. Scherman, *Chem. Rev.* **2015**, *115*, 12320–12406.
[26] J. Lagona, P. Mukhopadhyay, S. Chakrabarti, L. Isaacs, *Angew. Chem. Int. Ed.* **2005**, *44*, 4844–4870, *Angew. Chem.* **2005**, *117*, 4922–4949.
[27] R. P. Bosmans, W. E. Hendriksen, M. Verheijden, R. Eelkema, P. Jonkheijm, J. H. van Esch, L. Brunsveld, *Chem. Eur. J.* **2015**, *21*, 18466–18473.
[28] Q. An, J. Brinkmann, J. Huskens, S. Krabbenborg, J. de Boer, P. Jonkheijm, *Angew. Chem. Int. Ed.* **2012**, *51*, 12233–12237, *Angew. Chem.* **2012**, *124*, 12399–12403.
[29] S. Sankaran, E. Cavatorta, J. Huskens, P. Jonkheijm, *Langmuir* **2017**, *33*, 8813–8820.
[30] S. Sankaran, J. van Weerd, J. Voskuhl, M. Karperien, P. Jonkhejm, *Small* **2015**, *11*, 6187–6196.
[31] A. Gonzalez-Campo, M. Brasch, D. A. Uhlenheuer, A. Gomez-Casado, L. Yang, L. Brunsveld, J. Huskens, P. Jonkheijm, *Langmuir* **2012**, *28*, 16364–16371.
[32] S. Sankaran, L. Jaatinen, J. Brinkmann, T. Zameblli, J. Vörös, P. Jonkheijm, *ACS Nano* **2017**, *11*, 3867–3874.
[33] M. Wiemann, R. Niebuhr, A. Juan, E. Cavatorta, B. J. Ravoo, P. Jonkheijm, *Chem. Eur. J.* **2018**, *24*, 813–817.
[34] J. J. Reczek, A. A. Kennedy, B. T. Halbert, A. R. Urbach, *J. Am. Chem. Soc.* **2009**, *131*, 2408–2415.
[35] J. Geng, F. Biedermann, J. M. Zayed, F. Tian, O. A. Scherman, *Macromolecules* **2011**, *44*, 4276–4281.
[36] X. Duan, Y. Zhao, A. Perl, E. Berenschot, D. N. Reinhoudt, J. Huskens, *Adv. Funct. Mater.* **2010**, *20*, 663–668.
[37] J. Garcia-Amoros, M. Diaz-Lobos, S. Nonell, D. Velasco, *Angew. Chem. Int. Ed.* **2012**, *51*, 12820–12823, *Angew. Chem.* **2012**, *124*, 12992–12995.
[38] C. Stoffelen, J. Voskuhl, P. Jonkheijm, J. Huskens, *Angew. Chem. Int. Ed.* **2014**, *53*, 3400–3404, *Angew. Chem.* **2014**, *126*, 3468–3472.
[39] C. J. Sobers, S. E. Wood, M. Mrksich, *Biomaterials* **2015**, *52*, 385–394.
[40] Y. Xia, E. Kim, X. M. Zhao, J. A. Rogers, M. Prentiss, G. M. Whitesides, *Science* **1996**, *273*, 347–349.
[41] J. Movilli, A. Rozzi, R. Ricciardi, R. Corradini, J. Huskens, *Bioconjugate Chem.* **2018**, *29*, 4110–4118.
[42] M. Z. Markarian, M. D. Moussallem, H. W. Jomaa, J. B. Schlenoff, *Biomacromolecules* **2007**, *8*, 59–64.
[43] D. Yoo, S. S. Shiratori, M. F. Rubner, *Macromolecules*, **1998**, *31*, 4309–4318.
[44] J. Brinkmann, *Dynamic bioactive surfaces for cells using cucurbiturils, University of Twente*, PhD Thesis **2016**.
[45] J. F. Young, H. D. Nguyen, L. Yang, J. Huskens, P. Jonkheijm, L. Brunsveld, *ChemBioChem* **2010**, *11*, 180–183.
[46] J. L. Wilbur, A. Kumar, H. A. Biebuyck, E. Kim, G. M. Whitesides, *Nanotechnology* **1996**, *7*, 452–457.
[47] Y. Xia, E. Kim, G. M. Whitesides, *Chem. Mater.* **1996**, *8*, 1558–1567.
[48] E. A. Appel, F. Biedermann, D. Hoogland, J. del Barrio, M. D. Driscoll, S. Hay, D. J. Wales, O. A. Scherman, *J. Am. Chem. Soc.* **2017**, *139*, 12985–12993.

Manuscript received: March 22, 2019
Revised manuscript received: May 21, 2019
Accepted manuscript online: May 22, 2019